DisAp-dependent striated fiber elongation is required to organize ciliary arrays

Domenico F. Galati,[1] Stephanie Bonney,[1] Zev Kronenberg,[2] Christina Clarissa,[3] Mark Yandell,[2] Nels C. Elde,[2] Maria Jerka-Dziadosz,[4] Thomas H. Giddings,[3] Joseph Frankel,[5] and Chad G. Pearson[1]

[1]Anschutz Medical Campus, Department of Cell and Developmental Biology, University of Colorado, Aurora, CO 80045
[2]Department of Human Genetics, University of Utah School of Medicine, Salt Lake City, UT 84112
[3]Molecular, Cellular and Developmental Biology, University of Colorado at Boulder, Boulder, CO 80309
[4]Department of Cell Biology, M. Nencki Institute of Experimental Biology, 02-093 Warsaw, Poland
[5]Department of Biological Sciences, University of Iowa, Iowa City, IA 52242

Cilia-organizing basal bodies (BBs) are microtubule scaffolds that are visibly asymmetrical because they have attached auxiliary structures, such as striated fibers. In multiciliated cells, BB orientation aligns to ensure coherent ciliary beating, but the mechanisms that maintain BB orientation are unclear. For the first time in *Tetrahymena thermophila*, we use comparative whole-genome sequencing to identify the mutation in the BB disorientation mutant *disA-1*. disA-1 abolishes the localization of the novel protein DisAp to *T. thermophila* striated fibers (kinetodesmal fibers; KFs), which is consistent with DisAp's similarity to the striated fiber protein SF-assemblin. We demonstrate that DisAp is required for KFs to elongate and to resist BB disorientation in response to ciliary forces. Newly formed BBs move along KFs as they approach their cortical attachment sites. However, because they contain short KFs that are rotated, BBs in disA-1 cells display aberrant spacing and disorientation. Therefore, DisAp is a novel KF component that is essential for force-dependent KF elongation and BB orientation in multiciliary arrays.

Introduction

Motile cilia are whiplike projections that generate hydrodynamic force. Cilia-generated fluid flow is required for symmetry breaking during embryogenesis, mucus clearance, cerebrospinal fluid flow, and the directed movement of unicellular organisms (Marshall and Kintner, 2008). One cycle of ciliary beating constitutes a power stroke and a subsequent recovery stroke. Thus, ciliary beating is directional, and to produce coherent fluid flow, multiple cilia must orient their beating along a common plane, which is typically the cell's anterior–posterior axis. The importance of proper cilia orientation is underscored by the observation that cilia orientation defects accompany primary cilia dyskinesias, a devastating class of genetic disorders (Rayner et al., 1996).

Cilia are organized by cylindrical microtubule scaffolds called basal bodies (BBs) that dock at the cell cortex (Jana et al., 2014). BBs are innately asymmetric and their polarity is reflected in the attachment of auxiliary structures, including striated fibers (Allen, 1969; Pearson, 2014). Thus, BBs have a specific orientation that determines the direction of ciliary beating (Tamm et al., 1975; Gibbons, 1981; Hoops et al., 1984). BBs with improper orientation relative to the cellular anterior–posterior axis will disrupt cilia-generated fluid flow. The mechanisms that organize and maintain BB orientation remain ill-defined.

Striated fibers project asymmetrically from BBs and influence BB positioning by an unknown mechanism (Allen, 1967; Wright et al., 1983; Hoops et al., 1984). SF-assemblin and rootletin are coiled-coil proteins that self-organize into filamentous fiber structures and constitute major structural components of striated fibers in protists and vertebrates, respectively (Lechtreck and Melkonian, 1991; Yang et al., 2002), although other proteins are also present (Lechtreck and Melkonian, 1998; Park et al., 2008; Chien et al., 2013). Moreover, striated fibers display dynamic assembly and disassembly (Salisbury et al., 1984; Sperling et al., 1991; Francia et al., 2012). Thus, striated fibers are complex

Correspondence to Chad G. Pearson: Chad.Pearson@ucdenver.edu

Abbreviations used in this paper: BB, basal body; KF, kinetodesmal fiber; PEO, polyethylene oxide; TEM, transmission electron microscopy; WT, wild type.

The Rockefeller University Press $30.00
J. Cell Biol. Vol. 207 No. 6 705–715
www.jcb.org/cgi/doi/10.1083/jcb.201409123

and dynamic structures of which our molecular understanding is limited.

Unicellular ciliates, such as *Tetrahymena thermophila*, and multiciliated vertebrate cells harbor hundreds of cilia organized into ciliary arrays. Ciliary array BBs exhibit evolutionarily conserved striated fiber placement directly opposite the cilium's power stroke (Allen, 1969; Peraldi-Roux et al., 1991; Frankel, 1999). The *Tetrahymena* striated fiber, the kinetodesmal fiber (KF), emanates close to the BB's base and terminates within or directly underneath the membrane-skeletal layer near the adjacent anterior BB (Allen, 1967, 1969). The apposition of the KF and the postciliary microtubules from the anterior BB supports speculation that KFs stabilize ciliary rows by providing a physical linkage between neighboring ciliary units and by linkage to subcortical structures (Allen, 1967; Iftode and Fleury-Aubusson, 2003; Wloga and Frankel, 2012). Although this hypothesis has been strengthened by observations in *Chlamydomonas reinhardtii* (Wright et al., 1983; Hoops et al., 1984), a mechanistic understanding of how striated fibers organize ciliary arrays and respond to and resist mechanical forces has not been established.

Results and discussion

DisAp localizes to KFs and orients BBs

disA-1 is a single-locus, recessive mutation generated in a mutagenesis screen for *T. thermophila* BB organization defects (Frankel, 1979, 2008; Jerka-Dziadosz et al., 1995). *DISA* organizes BBs into ciliary rows, but is dispensable for global cellular polarity and for ciliogenesis (Fig. 1 A; Jerka-Dziadosz et al., 1995). The *disA-1* gene was identified using comparative genome sequence analysis with next-generation sequencing (Fig. S1, A and C). This approach identified a splice acceptor site mutation in intron 1 of a novel gene (TTHERM_00941400), which results in a severely truncated protein (Fig. 1 B and Fig. S1 B). The gene encodes a protein (DisAp) containing a similarity to the SF-assemblin consensus domain (Fig. 1 C; Lechtreck and Melkonian, 1998). Although the faint resemblance to SF-assemblin alerted us to a potential role in KF structure (pfam06705; BLASTp query of the Conserved Domain Database), phylogenetic analysis revealed that DisAp is a member of a distinct family of proteins conserved among ciliates, with seven paralogues in *T. thermophila*. Although this family includes other proteins with proposed roles in BB function (i.e., Bbc29p and Bbc39p; Kilburn et al., 2007), it does not include SF-assemblin. Therefore any shared function between DisAp and SF-assemblin may reflect convergent evolution, similar to previous observations for dynamin-like proteins in ciliates and metazoans (Elde et al., 2005). Introduction of TTHERM_00941400 into disA-1 cells rescues BB disorganization (Fig. 1 D). Thus, BB disorganization in *disA-1* is caused by the mutation of DisAp. Moreover, our discovery of DisAp provides proof-of-principle for the combined use of *Tetrahymena* forward genetic screens and next-generation sequencing to identify novel BB mutants.

SF-assemblin is the major component of algal striated fibers (Lechtreck and Melkonian, 1991). Striated fibers in *Paramecium tetraurelia* are composed of multiple polypeptides (Sperling, 1989), suggesting that the family of SF-assemblin genes expanded in ciliates. Indeed, *DISA* belongs to a family of genes that has undergone frequent duplications, especially evident in *P. tetraurelia*, and appears to be conserved in *Giardia*, a lineage distantly related to ciliates (Fig. S1 D and Table S1). However, SF-assemblin from *C. reinhardtii* does not associate with the clade, as assessed by reciprocal BLAST searches that failed to recover identity between these proteins (unpublished data). Therefore, to test whether DisAp localizes to *T. thermophila* KFs, wild-type (WT) GFP-DisAp and mutant disA-1 GFP-disA-1p were localized relative to BBs and KFs in otherwise WT cells. GFP-DisAp localizes to punctae along ciliary rows that colocalize with the proximal portion of the KF (Fig. 1, E and F). In contrast, mutant GFP-disA-1p does not localize to KFs (Fig. 1 E). GFP-DisAp is restricted to ciliary row BBs and is absent from oral apparatus BBs (Fig. 1 E, arrows), which form normally in disA-1 cells (Fig. 1 D, arrows).

DisAp's localization near the base of the KF suggested that it localizes to a discrete domain within the KF. Endogenously tagged DisAp-mCherry also localizes to the proximal portion of the KF (Fig. 1 F). Signal for DisAp is anterior to BBs and decreased below 50% ∼500 nm before KF intensity declined to 50%. Consistently, DisAp localized by immuno-EM clustered near the base of the KF (Fig. 1 G, yellow arrows; and Fig. S1 E). We also detected DisAp adjacent to the KF (Fig. 1 G, white arrows), which may reflect a population that has not incorporated into the KF. Thus, DisAp localizes to a domain at the proximal portion of the KF and is phylogenetically distinct from SF-assemblin.

DisAp loss disrupts BB orientation and prevents temperature-induced KF elongation

In disA-1 cells, KFs are disoriented relative to the cellular anterior–posterior axis. Therefore, DisAp could either specify the location of KF attachment to BBs or prevent BB rotation. Normally, KFs from adjacent BBs are aligned along a common axis and are oriented ∼180° from postciliary microtubules (Fig. 2 A; Allen, 1969). This KF placement is analogous to vertebrate BBs where the basal foot microtubules are positioned ∼180° from the striated rootlet (Steinman, 1968; Peraldi-Roux et al., 1991). In disA-1 cells, KFs are positioned ∼180° from the postciliary microtubules (Fig. 2 A), which suggests that DisAp prevents BB rotation and does not affect accessory structure placement. Moreover, disA-1 KFs are shorter than WT KFs (Fig. 2 A). Thus, DisAp prevents BB rotation and is required to establish and/or maintain appropriate KF length. We propose that DisAp functions as a regulator of KF elongation.

BB orientation defects in disA-1 cells are exacerbated by elevated temperature (Fig. 2 B; Jerka-Dziadosz et al., 1995). Thus, short KFs might allow temperature-induced BB rotation. If true, long KFs should prevent BB rotation. One prediction from this inference is that KFs elongate at elevated temperatures to resist BB rotation. To test this, we developed a semiautomated image analysis routine to measure KF length as well as BB orientation, and we assessed these parameters after shifting G1-arrested cells to 37°C and releasing them into the cell

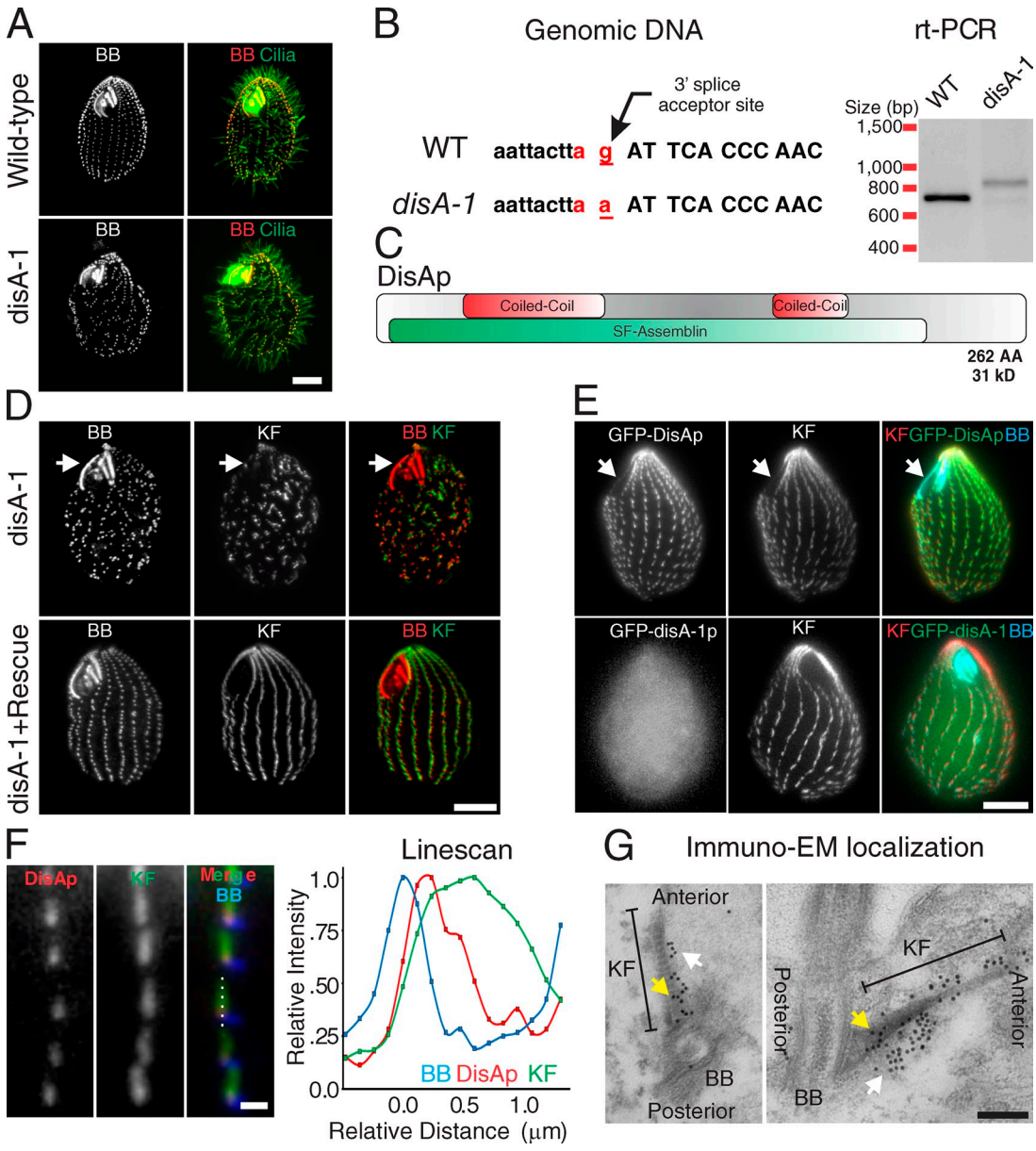

Figure 1. ***DISA* encodes a KF localizing protein.** (A) Disorganized BBs in *disA-1* mutants. BB (centrin; red) and cilia (α-tubulin; green) localization at 30°C is shown. (B) The *disA-1* mutation in Intron 1 of TTHERM_00941400. cDNA size increases due to the retained intron. (C) DisAp domain organization. (D) disA-1 phenotypes at 37°C are rescued with WT *DISA*. Arrows point to the location of the oral apparatus. (E) WT GFP:DisAp and mutant GFP:disA-1p localization relative to KFs and BBs. (F) DisAp-mCherry (red) localizes to the proximal portion of KFs (green). Shown on the right is a fluorescence intensity line scan of a single BB/KF unit. (G) Immuno-EM localization of DisAp-mCherry. Representative transverse (left) and longitudinal (right) sections are taken through a single BB. Yellow arrows point to gold particles associated with KF, and white arrows point to gold particles not associated with the KF. Bars: (A, D, and E) 10 μm; (F) 750 nm; (G) 200 nm.

cycle (Fig. 2 C). Before the temperature shift, WT cells had a mean KF length of 1.10 μm (Fig. 2 D). After the temperature shift, KF elongation reached 1.38 μm in length after 24 h (Fig. 2 D and Fig. S2 A). disA-1 KFs were approximately half as long (0.49 μm), and elongation was more gradual than in WT cells (Fig. 2 D and Fig. S2 B). Unlike WT, disA-1 cells displayed a time-dependent randomization of BB orientation (Fig. 2, E and F; and Fig. S2, C and D). These experiments were performed after a starvation-induced G1 arrest. Because starvation affects cortical organization (Nelsen and Debault, 1978), this could complicate our analyses. However, increased temperature in cycling cells that were not synchronized in G1 also caused WT KF elongation (Fig. 3, A and B) and increased disA-1 BB disorientation (Fig. 3 C). Thus, increased temperature, and not starvation, promotes DisAp-dependent KF elongation and increases the severity of BB disorientation in disA-1 cells. Collectively, these data uncover a novel relationship between KF length and BB orientation. First, the KF is dynamic and elongates in response to elevated temperature. Second, normal KF length requires DisAp. When the KF length is impaired, BBs are susceptible to rotation. We next investigated how temperature induces these changes in BB morphology.

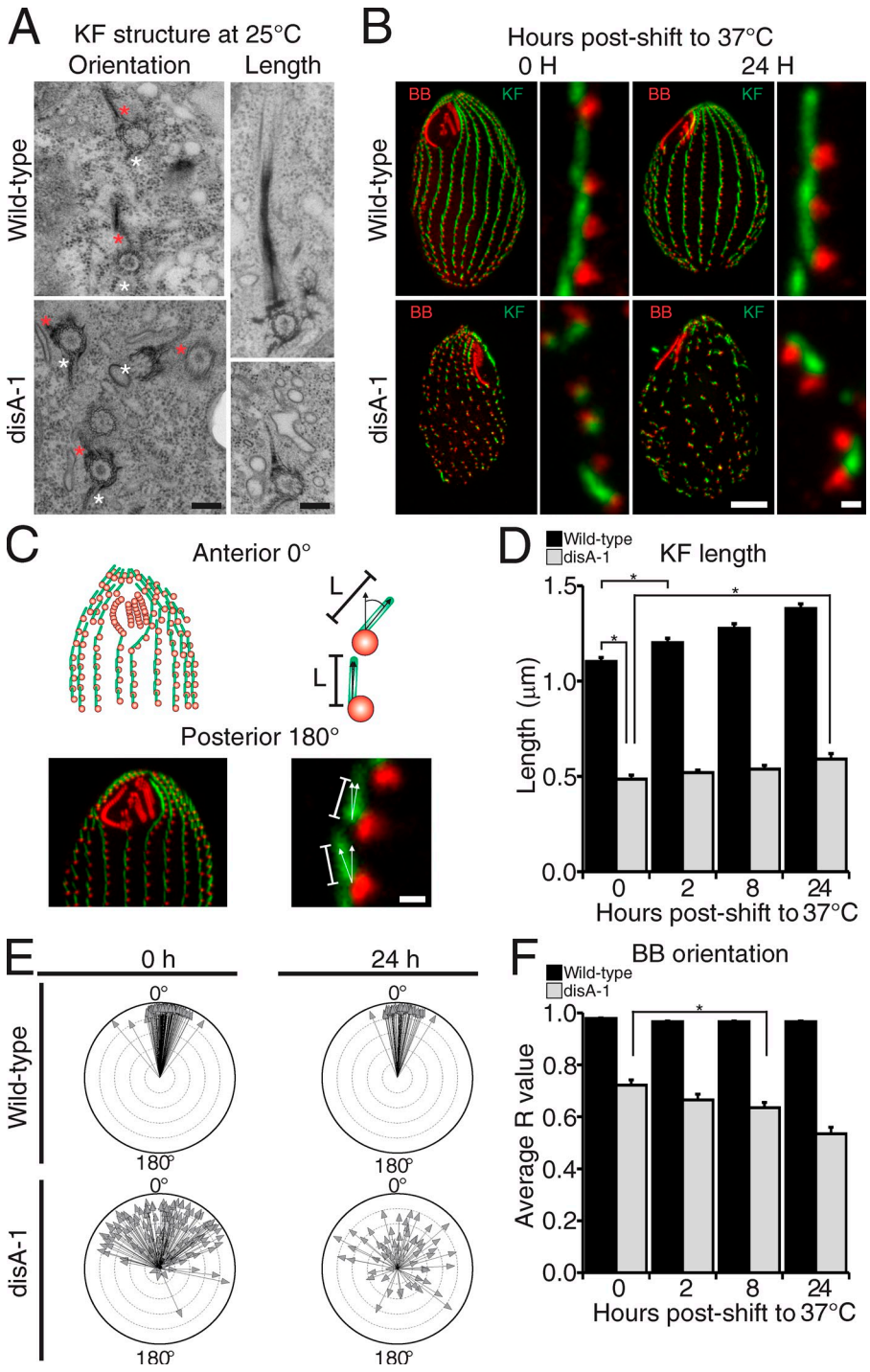

Figure 2. **Elevated temperature lengthens WT KFs and disrupts disA-1 BB orientation.** (A) TEM of ciliary rows at 25°C. DisAp loss causes BBs to rotate and decreases KF length. Red and white asterisks mark KFs and postciliary microtubules, respectively. Bars, 200 nm. (B) BB disorientation increases in disA-1 cells at 37°C (BB, red; KF, green). Bars: (left panels) 10 µm; (enlarged panels) 750 nm. (C) Quantification of KF (green) length and BB (red) orientation. Angular measurements represent the angle between the anterior pole (0°) and the tip of the KF. Length (L) is the distance between the BB and the KF tip. (D) Elevated temperature temporally lengthens KFs. $n > 300$ KFs. (E) BB disorientation in disA-1 cells is temperature sensitive. Arrow direction represents the mean angular measurement (mean vector) for BB orientation within a cell and arrow length represents the R value (mean vector length) for all measured angles for that cell. $n > 100$. (F) Temperature-induced BB disorientation in disA-1 cells. $n > 100$. Brackets indicate the samples being compared and asterisks indicate statistical significance ($P < 0.01$). Error bars indicate SEM.

DisAp confers resistance to mechanical forces produced by ciliary beating

Elevated temperature increases cilia beat frequency and cell swimming speed (Goto et al., 1982; Pearson et al., 2009), which confers greater cilia-generated forces on BBs (Bayless et al., 2012). We explored whether temperature-induced increases in force in disA-1 corresponds with the observed BB disorientation by quantifying cellular swim speeds at differing temperatures (Fig. 3, D and E). At 25°C, WT cells swam at 272 µm/s; this increased to 392 µm/s after a 10-min incubation at 37°C (acute) but decreased to an intermediate level (315 µm/s) after prolonged 24-h incubation at 37°C (chronic). disA-1 cells at 25°C exhibited a reduced swimming rate relative to WT cells (123 µm/s). Acute temperature shift increased the velocity (228 µm/s). However, unlike WT cells, increased motility was not sustained, as chronic maintenance at 37°C decreased the swimming rate below that of disA-1 cells grown at 25°C. This motility defect parallels disA-1 BB disorganization, with prolonged growth at 37°C causing more severe BB disorientation. The initial increase in swim speed in disA-1 cells shifted to 37°C for 10 min (acute) is likely the result of increased beat frequency. However, prolonged exposure to increased beating forces may

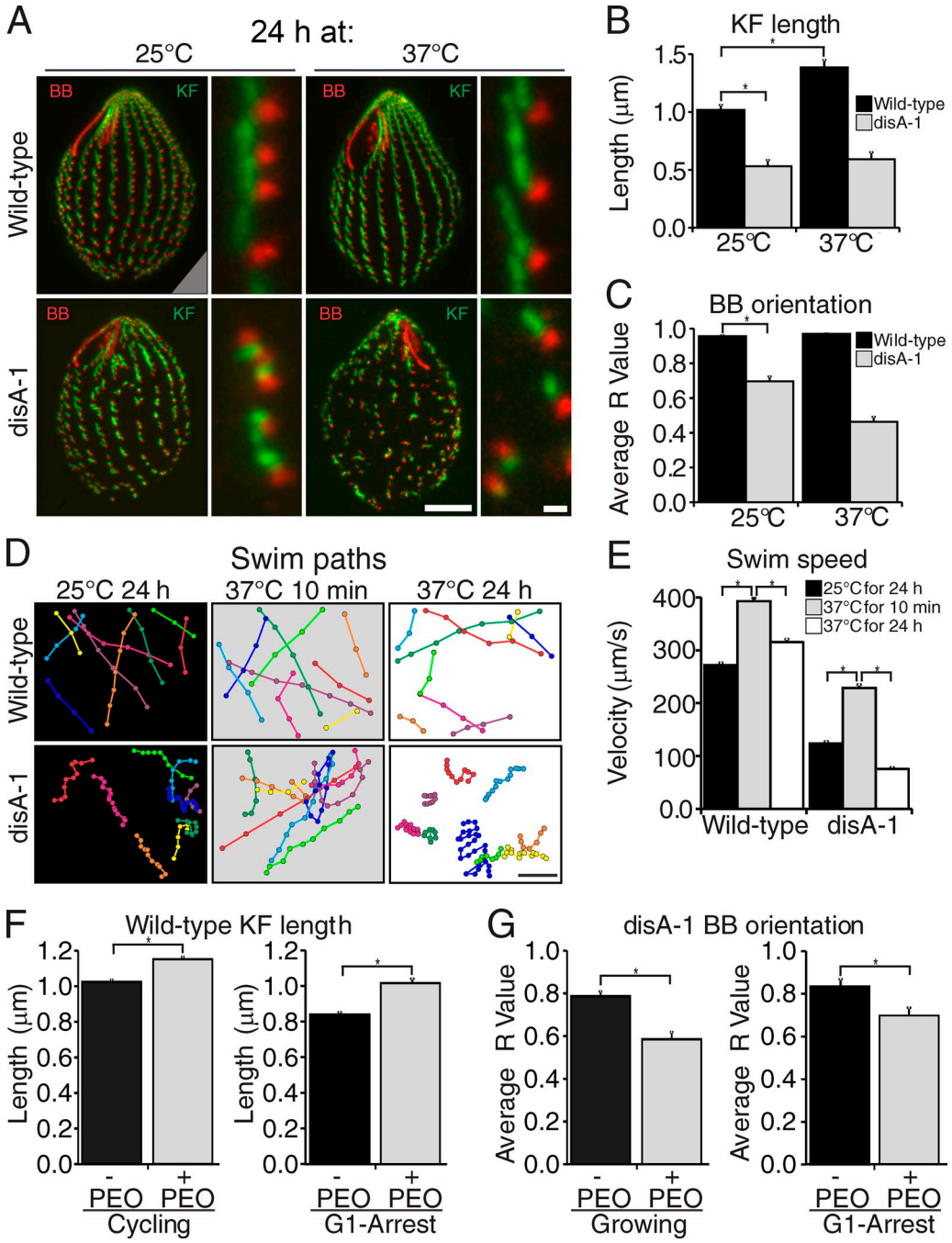

Figure 3. **Increased ciliary forces disorient BBs in disA-1 cells.** (A) Elevated temperature in cycling cells increases the disA-1 phenotype. BB, red; KF, green. Bars: (left panels) 10 µm; (enlarged panels) 750 nm. (B) Elevated temperature lengthens KFs. $n > 280$ KFs. (C) Elevated temperature increases disA-1 BB disorientation. $n > 54$. (D) Elevated temperature increases cell motility. The node spacing represents the distance traveled in 170 ms. Bar, 100 µm. (E) disA-1 cells do not maintain temperature-induced increases in motility. $n > 48$. (F and G) High-viscosity media lengthens WT KFs ($n > 153$ KFs) and disA-1 BB disorientation ($n > 30$) in cycling and G1-arrested cells grown in PEO at 25°C. Brackets indicate the samples being compared, and asterisks indicate statistical significance ($P < 0.01$). Error bars indicate SEM.

drive BB disorientation, thereby decreasing the effective rate of cell swimming.

Cilia-generated force increases WT KF length and disA-1 BB disorientation

We next tested whether increases in ciliary force influence KF elongation and BB orientation independent of temperature changes. The drag forces (physical resistance) that cilia experience can be increased by increasing their environmental viscosity with polymers (Spoon et al., 1977; Jung et al., 2014). In cycling cells cultured in high viscosity media (polyethylene oxide [PEO]) at 25°C, WT KFs elongated (Fig. 3 F) and disA-1 cells increased BB disorientation (Fig. 3 G). Moreover, high viscosity media also caused G1-arrested WT cells to undergo KF elongation (Fig. 3 F) and disA-1 cells to exhibit randomization of BB orientation (Fig. 3 G). Because G1-arrested cells

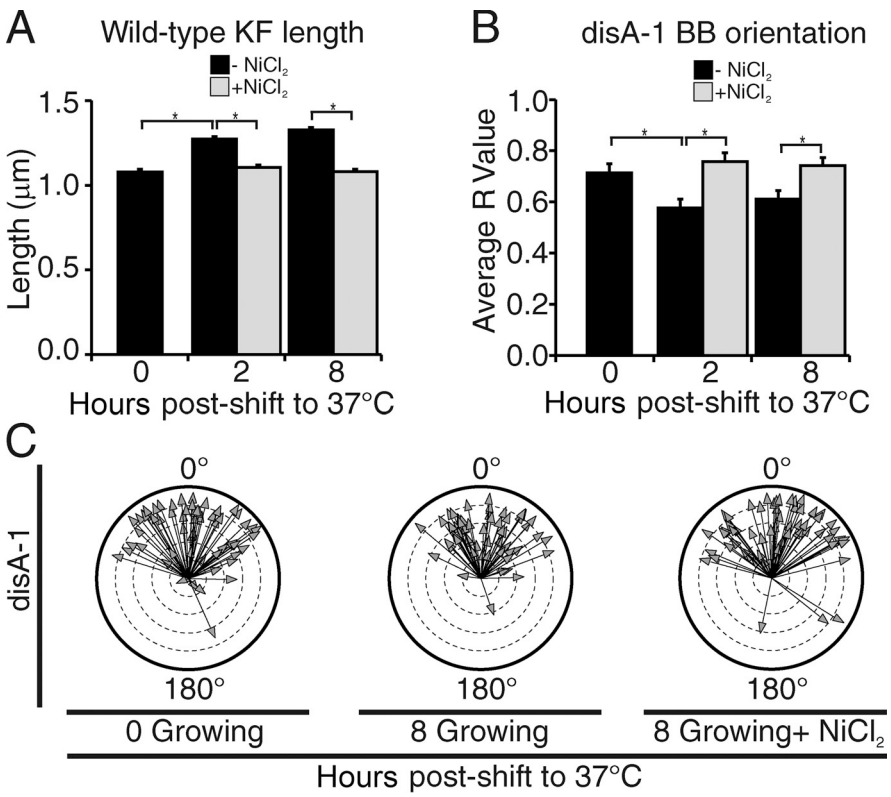

Figure 4. **Decreased cilia beating forces block KF elongation and rescue BB disorientation in disA-1 cells.** (A) Reduced ciliary beating prevents KF elongation. WT cells were grown at 37°C in $NiCl_2$. $n > 286$ KFs. (B) Reduced ciliary beating rescues temperature-induced BB disorientation in disA-1 cells. The circular R value is given for disA-1 cells grown as in A. $n > 56$. (C) Polar plots of the mean angular measurement for disA-1 cells where cilia beating was reduced. $n > 56$. Brackets indicate the samples being compared and asterisks indicate statistical significance ($P < 0.01$). Error bars indicate SEM.

do not assemble new BBs, BB assembly is not required for KF elongation or BB disorientation. Finally, increasing ciliary beat frequency with the cAMP agonist IBMX (Hennessey and Lampert, 2012) lengthened WT KFs and increased disA-1 BB orientation defects (Fig. S3, B and C), and when high temperature shift was accentuated with increased viscosity, an additive effect was observed (Fig. S3, D–F). Thus, increased ciliary-generated force triggers KF elongation. In the absence of KF elongation, as observed for disA-1, enhanced ciliary forces disrupts BB orientation.

Because cilia-generated force leads to KF elongation, we asked whether a reduction in ciliary beating prevents temperature-induced KF elongation. In the presence of $NiCl_2$ or vanadate, WT temperature-induced KF elongation at 2 and 8 h was abolished (Fig. 4 A and Fig. S3 G), which suggests that KFs elongate due to cilia-generated forces. Consistent with this, growth at 15°C slows cell swimming (Beveridge et al., 2010) and reduces KF length (Fig. S3 G). Moreover, the disorientation observed upon shifting disA-1 cells to 37°C was rescued by reducing ciliary beating with either $NiCl_2$ or vanadate (Fig. 4, B and C). Similarly, growth at 15°C slightly reduced disA-1 BB disorientation (Fig. S3 H; not statistically significant). Thus, cilia-generated force is both necessary and sufficient to increase BB disorientation in disA-1 cells, and BB rotation is resisted by DisAp-mediated KF elongation.

KFs guide nascent BBs and maintain the position of mature BBs

KFs terminate subjacent to the cortical membranes in the membrane-skeletal layer, where stable attachment of the KF may stabilize BBs against rotation. To determine whether KF elongation increases contacts between the KFs and the membrane-skeletal layer, we used three-dimensional image averaging to determine the mean length of the KF that lies near to the cell cortex. This position is defined by centrin, which marks the distal end of the BB near the membrane-skeletal layer (Stemm-Wolf et al., 2005). In WT cells at 25°C, the KF full-width at half maximum (FWHM) intensity above the plane of centrin was 1.09 µm long, which increased to 1.28 µm upon shifting to 37°C for 24 h (Fig. 5 A). In disA-1 cells cultured at 25°C, the KF FWHM was 0.57 µm, and it decreased to 0.51 µm after shifting to 37°C (Fig. 5 B). These results argue that force-dependent KF elongation augments the contact between the KF and anchoring structures in the cell cortex.

BB orientation in ciliates is propagated via a nongenetic process termed cytotaxis, which relies upon preexisting structures, such as old BBs, to constrain the position and orientation of newly arising structures, such as new BBs (Sonneborn, 1964; Beisson and Sonneborn, 1965; Beisson, 2008). Interactions between BBs and KFs or striated rootlets are proposed to organize the even spacing of BBs (Allen, 1969; Wright et al., 1983; Hoops et al., 1984; Lechtreck et al., 2002; Iftode and Fleury-Aubusson, 2003). In ciliates, these interactions occur between the KF and the postciliary microtubules of adjacent BBs in a ciliary row (Fig. 5 C). Nascent BBs are assembled at a mother BB and then transported along the mother BB's KF to separate the daughter from the mother (Fig. 5 C). In disA-1, the association between neighboring BBs and the KF is generally preserved (Fig. 5 D), which suggests that DisAp is not essential to link adjacent BBs to the KF. However, because disA-1 KFs are short and disoriented with respect to the cellular anterior–posterior axis, BB separation along the KF leads to clusters of closely spaced BBs

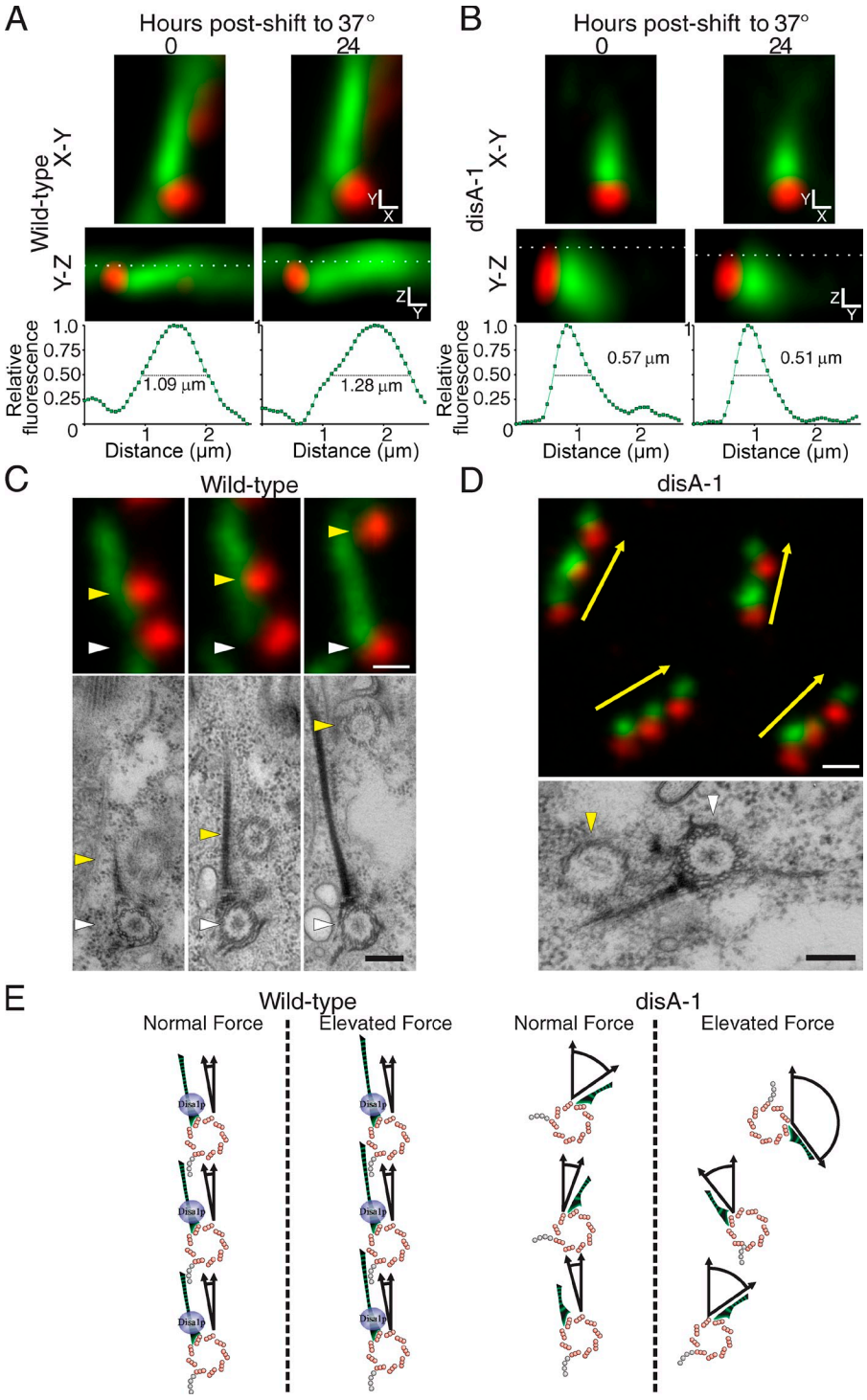

Figure 5. **The KF guides and maintains the position of nascent BBs.** (A and B) Averaged images showing increased KF presence near the membrane-skeletal layer after force-dependent elongation. Shown is the average KF signal (green) at the plane of the cell (broken line) orthogonal to the 90th percentile of centrin BB signal (red). Normalized line scans of fluorescence intensity along the broken line are shown. (C) BBs traverse the KF as they separate from their mother. (C, top) Fluorescence images. White arrowheads, mother BB. Yellow arrowheads, daughter BB. (C, bottom) TEMs representing BB separation. Bar, 200 nm. (D) The association between BBs and KFs is retained in disA-1 cells. (D, top) Shortened and disoriented KFs organize closely spaced BBs aligned along a common, but disoriented, axis (yellow arrows). (D, bottom) EM of a daughter BB (yellow arrowhead) associated with a parent BB (white arrowhead) in a disA-1 cell. (E) WT BBs are oriented along the cellular anterior–posterior axis. When force increases, the KF lengthens in a DisAp-dependent manner, which prevents BB rotation. disA-1 BBs are disorganized, but generally polarize along the cellular anterior–posterior axis. When force increases, KFs do not elongate, leading to force-dependent BB rotation and severe BB disorientation. Bars: (A and B); 320 nm; (C, top) 750 nm; (C, bottom) 200 nm; (D, top) 1.5 µm; (D, bottom) 200 nm.

oriented along a shared axis, each of which deviates from the cellular polarity (Fig. 5 D). Thus, similar to striated fiber-dependent centrosome cohesion and daughter cell positioning (Bahe et al., 2005; Francia et al., 2012), KFs actively position BBs in multiciliary arrays. Moreover, by ensuring that KFs reach an appropriate length, which prevents BB rotation, DisAp allows cytotaxis to perpetuate accurate cortical patterning.

We show that the KF is a major component of the structural environment into which nascent BBs are born. In addition, a genetic input, *DISA*, is required to maintain this environment. We have identified situations (DisAp-deficient) in which cilia-generated forces weaken and partially abolish cytotaxis. This expands upon the concept of structural inheritance to demonstrate that it is both plastic and subservient to the forces that act on BBs.

Conclusion

We demonstrate that the length of the striated fiber in *T. thermophila*, the KF, is responsive to forces generated by cilia. Furthermore, KF elongation stabilizes BB orientation, ensuring

ciliary alignment and coherent fluid flow. Through next-generation sequencing, we identified *DISA* as a gene responsible for BB organization whose protein is required for KF elongation. Finally, the stability of BB orientation and KF length are important for the propagation of the structural order in cells.

How the forces generated by cilia are sensed and then translated into KF length regulation remains to be determined, and the site of force detection, whether it be the BB or the KF, is also unknown. Because DisAp localizes near the BB and is important for KF elongation, it is an attractive target for force response. Furthermore, our results extend beyond cortical patterning in ciliates. In vertebrates, the striated rootlet, which is analogous to the KF, plays a prominent role in stabilizing the orientation of the ciliary unit (Chien et al., 2013). Therefore, our study raises the intriguing possibility that force sensing and response by BB-associated striated fibers is a conserved mechanism that has independently evolved in different eukaryotic lineages to couple ciliary forces to BB orientation.

Materials and methods

Tetrahymena culture

T. thermophila cells were grown in 2% SPP media (2% proteose peptone, 0.2% glucose, 0.1% yeast extract, and 0.003% Fe-EDTA) at the indicated temperatures (either 15°, 25°C, or 37°C). For all cycling cell studies, cells were analyzed at mid-log phase (density between 10^5 and 4×10^5 cells/ml) as determined using a Coulter Counter Z1 (Beckman Coulter). For starvation experiments, cells were arrested in the G1 phase of the cell cycle by washing and culturing in 10 mM Tris-HCl, pH 7.4, for 18–24 h. For microscopy experiments, analyses were restricted to nondividing cells as judged by those lacking an oral primordium. To expose cells to increased viscosity, *Tetrahymena* were propagated in 2× SPP supplemented with an equal volume of 7.5% polyethylene oxide (mol wt 900,000; Acros Organics), which was prepared in ddH_2O by gentle mixing at 37°C for 24–48 h. Alternatively, 2% SPP was supplemented with 750 nm of the phosphodiesterase inhibitor 3-isobutyl-1-methylxanthine (IBMX; Sigma-Aldrich), which increases cAMP levels and cilia beat frequency. To expose cultures to decreased forces, *Tetrahymena* were propagated in 2% SPP supplemented with 250 µm $NiCl_2$ (Sigma-Aldrich), which was added directly to the culture vessel from a 5-M stock. Dynein-dependent ciliary beating is inhibited by $NiCl_2$, which blocks plasma membrane calcium channels and directly inhibits dynein motors (Larsen and Satir, 1991). Alternatively, 2% SPP was supplemented with 750 µm sodium orthovanadate (Sigma-Aldrich; Gibbons et al., 1978; Nilsson, 1999), which was added directly to the culture vessel from a 100-mm stock (pH 10).

Plasmids and *Tetrahymena* strain construction

To rescue the disA-1 phenotype with WT *DISA*, disA-1 cells (IA217) were transformed with the *DISA* ORF, and flanking sequences were inserted exogenously into the genome at *RPL29*. Specifically, *DISA* was PCR amplified from WT (B2086) cells using oligos (5′-CGCTGCAGAAAGATAGATGCTTGCTTGC-3′ and 5′-CGGAGCTCGCTGTATTCTAAAGTTCAAG-3′) and cloned into pBSMCSCHX. After release with Blp1 digest, the rescue construct was biolistically transformed into disA-1 cells and selected for cycloheximide resistance and rescue of the disA-1 phenotype.

GFP-DISA and GFP-disA-1 were cloned into pNEO2-MTTpr-GFP that inserts an MTT-GFP cassette upstream of the endogenous gene (Winey et al., 2012). The cassette containing either WT or *disA-1* mutant sequence was inserted into otherwise WT cells. 0.6 kb of sequence upstream of *DISA* was PCR amplified (5′-CGGAGCTCCTGTTTAAAATTAAGCATGCTC-3′ and 5′-CGGGATTCGCCTTATTAACCGTTTCCTT-3′) and cloned into pNEO2-MTTpr-GFP. Next, a 0.6-kb sequence of either DISA or disA-1 was PCR amplified (5′-CGCTCGAGATGTCTGCTTTCGGCTCTCC-3′ and 5′-CGGGGCCCCTTAATTTCTTTACCCTTTC-3′) and cloned into the plasmid to produce either pNEO2-MTT-GFP-DISA or pNEO2-MTT-GFP-disA-1.

A DisAp-mCherry strain was constructed. The p4T2-1:DisA:mCherry cassette integrates at the endogenous *DISA* locus and remains under the control of the endogenous promoter. p4T2-1:DISA:mCherry was generated by PCR amplifying (5′-CGGGATCCAAAATTGCAACTATCTAAAC-3′ and 5′-CGGAGCTCTCAAGTGAGCTTTAACTATC-3′) and cloning the final 0.6 kb of *DISA* without the TGA stop codon into p4T2-1-mCherryLAP (Winey et al., 2012). A 0.9-kb fragment downstream of the TGA stop codon (5′-CGGGTACCAGAAAATCATATTGAAACAC-3′ and 5′-CGGAATTCTTGACGGAAGTTCTTATCAATTCTCTAGCAAGTG-3′) was then cloned into the plasmid to create p4T2-1:DISA:mCherry. This plasmid contains NEO2 drug selection.

Next-generation sequencing and identification of disA-1

To generate a backcross of the *disA-1* mutation, IA217 (*disA-1*) and B1868 (WT) *Tetrahymena* lines were crossed to produce micronuclear heterozygous F1 progeny. Two F1 clones of different mating types (F1.1 and F1.8) were then mated to produce 18 F2 *disA-1* mutant lines. Total genomic DNA was purified from each line using a urea-SDS lysis and phenol:chloroform extraction (Gaertig et al., 1994) and measured using a Qubit Fluorometer (Invitrogen). Equal DNA was pooled for all 18 F2 clones to produce a single Illumina Tru-seq library. A second DNA preparation of B1868 was also prepared. Using Illumina's standard TruSeq DNA library preparation, DNA was first sheared to a 300–400-bp distribution using sonication, and then end-repaired and A-tailed using a combination of T4 polynucleotide kinase (PNK), T4 DNA polymerase, and Klenow. A-tailed DNA was then ligated to Illumina Truseq adapters, and further independently indexed using PCR. Both libraries were size selected to remove adapter and PCR dimers, pooled, and co-sequenced on a single lane of the Illumina HiSeq 2000 using a 2 × 100 base pair format. Postsequencing bioinformatics were used to separate sequences from each of the two libraries using the unique indexes incorporated during the library process.

The pipeline for mapping and variant calling in the data are reported in a publicly available Wiki (https://github.com/jewmanchue/pooled-mapping). To improve read quality, 10 and 5 bp were trimmed from the 5′ and 3′ ends, respectively. Reads were locally aligned simultaneously to two reference sequences (micronucleus: tetrahymena_thermophila_sb210__mic__2_supercontigs; and macronucleus: JCVI-TTA1-2.2) using bowtie-2.0.0. (Langmead and Salzberg, 2012). Discordant mate pairs were discarded. The reads mapped to the genome were >98% for B1868 control and >95% for the *disA-1* F2. Sequencing coverage for the entire genome was 0.96 and 0.60 for the B1868 and *disA-1* strains, respectively. Alignment cleanup was performed using Samtools to remove PCR duplicates GenomeAnalysisTK-2.4-7 was used to realign indels and polish alignments (Li et al., 2009; McKenna et al., 2010; DePristo et al., 2011). Joint variant calling for the *disA-1* F2 and the B1868 control pool was performed using SNVerPool (Wei et al., 2011).

Heuristic filters were applied to the 8,795,723 mutations (SNVs, 7,346,955; insertions, 648,913; deletions, 799,855) using the Genotype-Phenotype Association Toolkit (https://github.com/jewmanchue/vcflib/wiki). Positions in the genome with a depth <5 in the B1868 or *disA-1* mutant pools were removed. The second filter removed positions where the B1868 pool contained the nonreference allele. The last filter leniently enforced a recessive model by requiring the frequency of the nonreference allele in the *disA-1* mutant pool to be >0.75. A filter of 0.75 was used to avoid false negatives created from sequencing errors. However, the *disA-1* mutation did have an allele frequency of 1.0. After filtering, only 206 mutations were remaining, 26 of which were homozygous nonreference (allele frequency of one) in the *disA-1* mutant pool (Fig. S1 C). We focused on the nine mutations mapped to the macronuclear sequence. Nine candidate positions for the *disA-1* mutation were identified and narrowed down by searching for proteins containing domains commonly associated with BBs and their auxiliary structures. Hand annotation revealed that one of the mutations was a splice site mutation in the 3′ acceptor site (G to A) in TTHERM_00941400. This mutation was found in both the macronuclear and micronuclear sequences. The mutation was also confirmed by both PCR of the genomic region and cDNA of TTHERM_00941400 and sequencing.

Phylogenetic analysis

The amino acid sequence of DisAp from *T. thermophila* (XP_001026900) was used in a protein–protein blast query (http://www.ncbi.nlm.nih.gov) to identify related sequences (Table S1). Alignments were generated with ClustalW2 (http://www.ebi.ac.uk) and trimmed by eye to eliminate insertions and deletions. Model fitting and tree inference of the alignment was performed with Mr. Bayes v3.2.2 (Ronquist and Huelsenbeck, 2003). The "rtrev" amino acid substitution model was best supported by the data and used for inferring the tree. After the burn-in phase, the remainder of 500,000 generations of Markov chain Monte Carlo analysis were considered for

inference of the tree. The 50% majority rule consensus tree was generated and visualized with FigTree v1.4.

Immunocytochemistry

For immuno-cytochemical analyses, 1–3 × 10^5 cells were pelleted at 1,500 *g* in a 1.5-ml Eppendorf tube and fixed for 20–30 min with 1.5 ml of 70% ethanol + 0.2% Triton X-100. Cells were washed with 10 mM Tris-buffered saline and blocked overnight at 4°C in 1% BSA in 10 mM TBS. Cells were immunostained by incubating overnight at 4°C in primary antibody (mouse anti-KF [5D8], 1:400; Jerka-Dziadosz et al., 1995; rabbit anti-centrin, 1:2,000, a gift from A. Stemm-Wolf and M. Winey, University of Colorado Boulder, Boulder, CO; Stemm-Wolf et al., 2005; rabbit anti–α tubulin, DM1a; Sigma-Aldrich) followed by a 1-h incubation at room temperature in secondary antibody (goat anti–mouse Alexa Fluor 594, 1:2,000; goat anti–rabbit Alexa Fluor 488, 1:2,000; goat anti–Alexa Fluor 647, 1:2,000; Invitrogen). Cells were mounted in Citifluor mounting media (Citifluor LTD) using #1.5 coverslips and sealed with nail polish. All antibodies were diluted in 1% BSA/TBS. Cells were washed (3 × 5 min) with 1% BSA/TBS after primary and secondary antibody incubations.

Light microscopy

For the localization experiments in Fig. 1, an inverted microscope (Ti Eclipse; Nikon) with a 100× Plan-Apochromat (NA 1.4) objective lens (Nikon) was used. Images were captured with an electron-multiplying charge-coupled device (EMCCD) 888E camera (iXon; Andor Technology). For all other experiments, confocal microscopy was performed using an inverted microscope (Ti Eclipse) with a 100× Plan-Apochromat (NA 1.43) objective lens (Nikon) and a Swept Field confocal scan head (Prairie Technologies). Confocal images were acquired in slit mode with a slit size of 35 µm and a z-step size of 200 nm, and detected with a charge-coupled device (CCD) camera (Clara; Andor Technology). Images were acquired with Elements software (Nikon) and all fixed cells were imaged at room temperature.

Transmission EM (TEM)

EM was performed as described previously (Pearson et al., 2009; Bayless et al., 2012). A *Tetrahymena* strain expressing endogenous C-terminal DisAp-mCherry was grown to mid-log phase and then prepared for immuno-EM using high-pressure freezing and freeze substitution (HPF-FS; Dahl and Staehelin, 1989; Meehl et al., 2009). *T. thermophila* cells were pelleted, high-pressure frozen (HPM-010; Bal-Tec), freeze substituted in 0.25% glutaraldehyde/0.1% uranyl acetate in acetone, and embedded in Lowicryl HM20. 60-nm serial sections were cut and put on nickel slot grids, blocked with 1% milk in PBS–Tween 20, and incubated with anti-mCherry (rabbit polyclonal; a gift from I. Cheeseman, Massachusetts Institute of Technology, Cambridge, MA) at 1:100. 15 nm of gold-conjugated secondary antibody was applied to the grids at a dilution of 1:20 (Ted Pella). Grids were poststained with 2% uranyl acetate and lead citrate.TtBld10 was then localized in 60-nm sections using TEM. Images were collected using a Philips CM10 electron microscope (Philips) equipped with a Gatan BioScan2 CCD camera (Gatan). For structural analyses of *disA-1* BB defects, *disA-1* and control (B1868) cells were subjected to HPF-FS after growth at 25°C.

***Tetrahymena* motility measurements**

Free-swimming *Tetrahymena* in glass-bottom dishes were imaged using a 20× objective lens (pixel size, 330 nm) and transmitted light on the confocal microscope (see "Light microscopy"). For each field of view, images were captured at ∼170-ms intervals for a total of 30 s. To track motility paths, we marked the anterior tip of individual *Tetrahymena* that displayed directional motility for the duration of their swim path while they remained in focus. Care was taken to avoid *Tetrahymena* at the glass surface. Tracking analysis was facilitated by the MTrackJ (Meijering et al., 2012) plugin bundled with FIJI (Schindelin et al., 2012).

Image analysis: KF length and BB orientation

KF length and BB orientation quantification were performed in a semiautomated fashion using the macro scripting language and plugins contained within the FIJI build of ImageJ. Image stacks were preprocessed with a Laplacian of Gaussian filter (LOG; radius, 1 pixel) to reduce noise and enhance feature edges. 32-bit LOG stacks were inverted, their contrast was adjusted (minimum = mode pixel intensity + (1/2) × standard deviation pixel intensity; maximum = maximum pixel intensity), and the images were merged to create an 8-bit RGB image stack. To quantify KF length for individual cells, 10 KFs with clear separation from neighboring KFs were manually measured by tracing with the freehand line tool. To quantify BB orientation, a box (10 µm wide × 5 µm tall) was placed in the center of a *Tetrahymena* cell and angular measurements were made for 10 BBs within that box. For each BB, the angular measurement represents the angle between the tip of the KF and the anterior pole of the cell (Fig. 2 C). For each cell, the mean vector and the length of the mean vector (R value) for the 10 measured BBs were calculated using circular statistics and displayed on polar plots. Each cell was measured twice, once on each side; thus each cell produced two R values. On the polar plots the mean vector is represented by the direction of the arrow. Variance in the mean vector is represented by the length of the arrow. An arrow length of 1 indicates no variation in the mean vector and an arrow length of 0 represents pure randomness in the mean vector. On the polar plots, the dashed circles represent 0.2 arbitrary units of R value. To compare the amount of BB orientation defects across different populations of cells, the mean R value for the cell population was determined in linear space. Circular statistics were calculated using the ORIANA circular statistics suite (Kovach Computing Services).

Image analysis: fluorescent image averaging

The brightest centrin (BB) voxel for an individual BB was determined. A 5-µm box was centered over this voxel in the x, y, and z dimensions. The raw BB and KF image stacks were cropped in the xy dimension using the 5-µm box, and they were cropped in the z dimension by taking five slices below the slice containing the brightest BB voxel and five slices above the brightest BB voxel (11 slices total; 3.3 µm). Next, cropped stacks were rotated so that the tip of the KF was aligned with a straight line that ran down the middle of the 5-µm box and passed through the brightest centrin pixel. This procedure was performed on 100 BBs from 10 different cells for each condition. The raw images used for averaging were part of the 0 h and 24 h time points (SPP condition) of the dataset used in Fig. S3 (D and E). To create the average image stack, individual image stacks were averaged on a per-slice basis. All image cropping was performed with FIJI using the crop, rotate, and duplicate stack commands. The yz images were created by rotating the averaged image stacks in three dimensions using the TransformJ plugin.

Statistical analysis

All linear statistical analyses were performed in Excel (Microsoft). All tests for significance were unpaired, two-tailed *t* tests. All error bars indicate SEM. Statistical significance was set at $P < 0.01$.

Online supplemental material

Fig. S1 shows the scheme used for the identification of the *disA-1* mutation, a phylogenetic tree of related DisAp proteins, and immuno-EM confirming DisAp's localization at the KF. Fig. S2 shows the frequency distributions of WT and disA-1 KF length and BB orientation upon temperature shift, which documents population-wide shifts in KF length and BB orientation. Fig. S3 shows that WT BBs are resistant to force-induced orientation defects, whereas additional force perturbations impact WT KF length and disA-1 BB orientation. Table S1 lists the *Tetrahymena DISA-1* clade members. Online supplemental material is available at http://www.jcb.org/cgi/content/full/jcb.201409123/DC1.

We thank Alex Stemm-Wolf and Dr. Brian Mitchell for comments on the manuscript. We thank Dr. Ken Jones, Joe Brown, Dr. Bifeng Gao, and Katrina Diener for providing sequencing and preliminary analyses.

The sequencing was supported by a pilot grant from the University of Colorado Denver Genomics and Microarray Core made possible by the Genomics and Biostatistics/Bioinformatics Shared Resources of Colorado's National Institutes of Health (NIH)/National Cancer Institute Cancer Center Support Grant P30CA046934. C.G. Pearson is supported by NIH-NIGMS GM0099820 and the Boettcher Webb-Waring Foundation. C.G. Pearson and N.C. Elde are supported by the Pew Biomedical Scholars Program.

The authors declare no competing financial interests.

Submitted: 25 September 2014
Accepted: 25 November 2014

References

Allen, R.D. 1967. Fine structure, reconstruction and possible functions of components of the cortex of *Tetrahymena pyriformis*. *J. Protozool.* 14:553–565. http://dx.doi.org/10.1111/j.1550-7408.1967.tb02042.x

Allen, R.D. 1969. The morphogenesis of basal bodies and accessory structures of the cortex of the ciliated protozoan *Tetrahymena pyriformis*. *J. Cell Biol.* 40:716–733. http://dx.doi.org/10.1083/jcb.40.3.716

Bahe, S., Y.-D. Stierhof, C.J. Wilkinson, F. Leiss, and E.A. Nigg. 2005. Rootletin forms centriole-associated filaments and functions in centrosome cohesion. *J. Cell Biol.* 171:27–33. http://dx.doi.org/10.1083/jcb.200504107

Bayless, B.A., T.H. Giddings Jr., M. Winey, and C.G. Pearson. 2012. Bld10/Cep135 stabilizes basal bodies to resist cilia-generated forces. *Mol. Biol. Cell*. 23:4820–4832. http://dx.doi.org/10.1091/mbc.E12-08-0577

Beisson, J. 2008. Preformed cell structure and cell heredity. *Prion*. 2:1–8. http://dx.doi.org/10.4161/pri.2.1.5063

Beisson, J., and T.M. Sonneborn. 1965. Cytoplasmic inheritance of the organization of the cell cortex in *Paramecium aurelia. Proc. Natl. Acad. Sci. USA*. 53:275–282. http://dx.doi.org/10.1073/pnas.53.2.275

Beveridge, O.S., O.L. Petchey, and S. Humphries. 2010. Mechanisms of temperature-dependent swimming: the importance of physics, physiology and body size in determining protist swimming speed. *J. Exp. Biol.* 213:4223–4231. http://dx.doi.org/10.1242/jeb.045435

Chien, Y.-H., M.E. Werner, J. Stubbs, M.S. Joens, J. Li, S. Chien, J.A.J. Fitzpatrick, B.J. Mitchell, and C. Kintner. 2013. Bbof1 is required to maintain cilia orientation. *Development*. 140:3468–3477. http://dx.doi.org/10.1242/dev.096727

Dahl, R., and L.A. Staehelin. 1989. High-pressure freezing for the preservation of biological structure: theory and practice. *J. Electron Microsc. Tech.* 13:165–174. http://dx.doi.org/10.1002/jemt.1060130305

DePristo, M.A., E. Banks, R. Poplin, K.V. Garimella, J.R. Maguire, C. Hartl, A.A. Philippakis, G. del Angel, M.A. Rivas, M. Hanna, et al. 2011. A framework for variation discovery and genotyping using next-generation DNA sequencing data. *Nat. Genet.* 43:491–498. http://dx.doi.org/10.1038/ng.806

Elde, N.C., G. Morgan, M. Winey, L. Sperling, and A.P. Turkewitz. 2005. Elucidation of clathrin-mediated endocytosis in *tetrahymena* reveals an evolutionarily convergent recruitment of dynamin. *PLoS Genet.* 1:e52. http://dx.doi.org/10.1371/journal.pgen.0010052

Francia, M.E., C.N. Jordan, J.D. Patel, L. Sheiner, J.L. Demerly, J.D. Fellows, J.C. de Leon, N.S. Morrissette, J.-F. Dubremetz, and B. Striepen. 2012. Cell division in Apicomplexan parasites is organized by a homolog of the striated rootlet fiber of algal flagella. *PLoS Biol.* 10:e1001444. http://dx.doi.org/10.1371/journal.pbio.1001444

Frankel, J. 1979. An analysis of cell-surface patterning in *Tetrahymena. Symp. Soc. Dev. Biol.* 37:215–246.

Frankel, J. 2000. Cell biology of *Tetrahymena thermophila. Methods Cell Biol.* 62:27–125. http://dx.doi.org/10.1016/S0091-679X(08)61528-9

Frankel, J. 2008. What do genic mutations tell us about the structural patterning of a complex single-celled organism? *Eukaryot. Cell*. 7:1617–1639. http://dx.doi.org/10.1128/EC.00161-08

Gaertig, J., T.H. Thatcher, L. Gu, and M.A. Gorovsky. 1994. Electroporation-mediated replacement of a positively and negatively selectable β-tubulin gene in *Tetrahymena thermophila. Proc. Natl. Acad. Sci. USA*. 91:4549–4553. http://dx.doi.org/10.1073/pnas.91.10.4549

Gibbons, I.R., M.P. Cosson, J.A. Evans, B.H. Gibbons, B. Houck, K.H. Martinson, W.S. Sale, and W.J. Tang. 1978. Potent inhibition of dynein adenosinetriphosphatase and of the motility of cilia and sperm flagella by vanadate. *Proc. Natl. Acad. Sci. USA*. 75:2220–2224. http://dx.doi.org/10.1073/pnas.75.5.2220

Gibbons, I.R. 1981. Cilia and flagella of eukaryotes. *J. Cell Biol.* 91:107s–124s. http://dx.doi.org/10.1083/jcb.91.3.107s

Goto, M., K. Ohki, and Y. Nozawa. 1982. Evidence for a correlation between swimming velocity and membrane fluidity of *Tetrahymena* cells. *Biochim. Biophys. Acta*. 693:335–340. http://dx.doi.org/10.1016/0005-2736(82)90440-0

Hennessey, T.M., and T.J. Lampert. 2012. Behavioral bioassays and their uses in *Tetrahymena. Methods Cell Biol.* 109:393–410. http://dx.doi.org/10.1016/B978-0-12-385967-9.00015-3

Hoops, H.J., R.L. Wright, J.W. Jarvik, and G.B. Witman. 1984. Flagellar waveform and rotational orientation in a *Chlamydomonas* mutant lacking normal striated fibers. *J. Cell Biol.* 98:818–824. http://dx.doi.org/10.1083/jcb.98.3.818

Iftode, F., and A. Fleury-Aubusson. 2003. Structural inheritance in *Paramecium*: ultrastructural evidence for basal body and associated rootlets polarity transmission through binary fission. *Biol. Cell*. 95:39–51. http://dx.doi.org/10.1016/S0248-4900(03)00005-4

Jana, S.C., G. Marteil, and M. Bettencourt-Dias. 2014. Mapping molecules to structure: unveiling secrets of centriole and cilia assembly with near-atomic resolution. *Curr. Opin. Cell Biol.* 26:96–106. http://dx.doi.org/10.1016/j.ceb.2013.12.001

Jerka-Dziadosz, M., L.M. Jenkins, E.M. Nelsen, N.E. Williams, R. Jaeckel-Williams, and J. Frankel. 1995. Cellular polarity in ciliates: persistence of global polarity in a disorganized mutant of *Tetrahymena thermophila* that disrupts cytoskeletal organization. *Dev. Biol.* 169:644–661. http://dx.doi.org/10.1006/dbio.1995.1176

Jung, I., T.R. Powers, and J.M. Valles Jr. 2014. Evidence for two extremes of ciliary motor response in a single swimming microorganism. *Biophys. J.* 106:106–113. http://dx.doi.org/10.1016/j.bpj.2013.11.3703

Kilburn, C.L., C.G. Pearson, E.P. Romijn, J.B. Meehl, T.H. Giddings Jr., B.P. Culver, J.R. Yates III, and M. Winey. 2007. New *Tetrahymena* basal body protein components identify basal body domain structure. *J. Cell Biol.* 178:905–912. http://dx.doi.org/10.1083/jcb.200703109

Langmead, B., and S.L. Salzberg. 2012. Fast gapped-read alignment with Bowtie 2. *Nat. Methods*. 9:357–359. http://dx.doi.org/10.1038/nmeth.1923

Larsen, J., and P. Satir. 1991. Analysis of $Ni^{(2+)}$-induced arrest of *Paramecium* axonemes. *J. Cell Sci.* 99:33–40.

Lechtreck, K.F., and M. Melkonian. 1991. Striated microtubule-associated fibers: identification of assemblin, a novel 34-kD protein that forms paracrystals of 2-nm filaments in vitro. *J. Cell Biol.* 115:705–716. http://dx.doi.org/10.1083/jcb.115.3.705

Lechtreck, K.-F., and M. Melkonian. 1998. SF-assemblin, striated fibers, and segmented coiled coil proteins. *Cell Motil. Cytoskeleton*. 41:289–296. http://dx.doi.org/10.1002/(SICI)1097-0169(1998)41:4<289::AID-CM2>3.0.CO;2-1

Lechtreck, K.-F., J. Rostmann, and A. Grunow. 2002. Analysis of *Chlamydomonas* SF-assemblin by GFP tagging and expression of antisense constructs. *J. Cell Sci.* 115:1511–1522.

Li, H., B. Handsaker, A. Wysoker, T. Fennell, J. Ruan, N. Homer, G. Marth, G. Abecasis, R. Durbin, and 1000 Genome Project Data Processing Subgroup. 2009. The Sequence Alignment/Map format and SAMtools. *Bioinformatics*. 25:2078–2079. http://dx.doi.org/10.1093/bioinformatics/btp352

Marshall, W.F., and C. Kintner. 2008. Cilia orientation and the fluid mechanics of development. *Curr. Opin. Cell Biol.* 20:48–52. http://dx.doi.org/10.1016/j.ceb.2007.11.009

McKenna, A., M. Hanna, E. Banks, A. Sivachenko, K. Cibulskis, A. Kernytsky, K. Garimella, D. Altshuler, S. Gabriel, M. Daly, and M.A. DePristo. 2010. The Genome Analysis Toolkit: a MapReduce framework for analyzing next-generation DNA sequencing data. *Genome Res.* 20:1297–1303. http://dx.doi.org/10.1101/gr.107524.110

Meehl, J.B., T.H. Giddings Jr., and M. Winey. 2009. High pressure freezing, electron microscopy, and immuno-electron microscopy of *Tetrahymena thermophila* basal bodies. *Methods Mol. Biol.* 586:227–241. http://dx.doi.org/10.1007/978-1-60761-376-3_12

Meijering, E., O. Dzyubachyk, and I. Smal. 2012. Methods for cell and particle tracking. *Methods Enzymol.* 504:183–200. http://dx.doi.org/10.1016/B978-0-12-391857-4.00009-4

Nelsen, E.M., and L.E. Debault. 1978. Transformation in *Tetrahymena pyriformis*: description of an inducible phenotype. *J. Protozool.* 25:113–119. http://dx.doi.org/10.1111/j.1550-7408.1978.tb03880.x

Nilsson, J.R. 1999. Vanadate affects nuclear division and induces aberrantly-shaped cells during subsequent cytokinesis in *Tetrahymena. J. Eukaryot. Microbiol.* 46:24–33. http://dx.doi.org/10.1111/j.1550-7408.1999.tb04580.x

Park, T.J., B.J. Mitchell, P.B. Abitua, C. Kintner, and J.B. Wallingford. 2008. Dishevelled controls apical docking and planar polarization of basal bodies in ciliated epithelial cells. *Nat. Genet.* 40:871–879. http://dx.doi.org/10.1038/ng.104

Pearson, C.G. 2014. Choosing sides—asymmetric centriole and basal body assembly. *J. Cell Sci.* 127:2803–2810. http://dx.doi.org/10.1242/jcs.151761

Pearson, C.G., D.P.S. Osborn, T.H. Giddings Jr., P.L. Beales, and M. Winey. 2009. Basal body stability and ciliogenesis requires the conserved component Poc1. *J. Cell Biol.* 187:905–920. http://dx.doi.org/10.1083/jcb.200908019

Peraldi-Roux, S., C. Klotz, B. Nguyen-Thanh-Dao, and J. Gabrion. 1991. A common epitope is shared by ciliary rootlets and cell-cell adherens junctions in ciliated ependymal cells. *J. Cell Sci.* 99:297–306.

Rayner, C.F., A. Rutman, A. Dewar, M.A. Greenstone, P.J. Cole, and R. Wilson. 1996. Ciliary disorientation alone as a cause of primary ciliary dyskinesia syndrome. *Am. J. Respir. Crit. Care Med.* 153:1123–1129. http://dx.doi.org/10.1164/ajrccm.153.3.8630555

Ronquist, F., and J.P. Huelsenbeck. 2003. MrBayes 3: Bayesian phylogenetic inference under mixed models. *Bioinformatics*. 19:1572–1574. http://dx.doi.org/10.1093/bioinformatics/btg180

Salisbury, J.L., A. Baron, B. Surek, and M. Melkonian. 1984. Striated flagellar roots: isolation and partial characterization of a calcium-modulated contractile organelle. *J. Cell Biol.* 99:962–970. http://dx.doi.org/10.1083/jcb.99.3.962

Schindelin, J., I. Arganda-Carreras, E. Frise, V. Kaynig, M. Longair, T. Pietzsch, S. Preibisch, C. Rueden, S. Saalfeld, B. Schmid, et al. 2012. Fiji: an open-source platform for biological-image analysis. *Nat. Methods*. 9:676–682. http://dx.doi.org/10.1038/nmeth.2019

Sonneborn, T.M. 1964. The differentiation of cells. *Proc. Natl. Acad. Sci. USA*. 51:915–929. http://dx.doi.org/10.1073/pnas.51.5.915

Sperling, L. 1989. Isolation and partial characterization of ciliary rootlets from *Paramecium tetraurelia*. *In* Cytoskeletal and Extracellular Proteins. P.D.U. Aebi, and P.D.J. Engel, editors. Springer Berlin, Heidelberg. 316–318.

Sperling, L., G. Keryer, F. Ruiz, and J. Beisson. 1991. Cortical morphogenesis in *Paramecium*: a transcellular wave of protein phosphorylation involved in ciliary rootlet disassembly. *Dev. Biol.* 148:205–218. http://dx.doi.org/10.1016/0012-1606(91)90330-6

Spoon, D.M., I.I. Feise CO, and R.S. Youn. 1977. Poly(ethylene oxide), a new slowing agent for protozoa. *J. Protozool.* 24:471–474. http://dx.doi.org/10.1111/j.1550-7408.1977.tb04779.x

Steinman, R.M. 1968. An electron microscopic study of ciliogenesis in developing epidermis and trachea in the embryo of *Xenopus laevis*. *Am. J. Anat.* 122:19–55. http://dx.doi.org/10.1002/aja.1001220103

Stemm-Wolf, A.J., G. Morgan, T.H. Giddings Jr., E.A. White, R. Marchione, H.B. McDonald, and M. Winey. 2005. Basal body duplication and maintenance require one member of the *Tetrahymena thermophila* centrin gene family. *Mol. Biol. Cell*. 16:3606–3619. http://dx.doi.org/10.1091/mbc.E04-10-0919

Tamm, S.L., T.M. Sonneborn, and R.V. Dippell. 1975. The role of cortical orientation in the control of the direction of ciliary beat in *Paramecium*. *J. Cell Biol.* 64:98–112. http://dx.doi.org/10.1083/jcb.64.1.98

Wei, Z., W. Wang, P. Hu, G.J. Lyon, and H. Hakonarson. 2011. SNVer: a statistical tool for variant calling in analysis of pooled or individual next-generation sequencing data. *Nucleic Acids Res.* 39:e132. http://dx.doi.org/10.1093/nar/gkr599

Winey, M., A.J. Stemm-Wolf, T.H. Giddings Jr., and C.G. Pearson. 2012. Cytological analysis of *Tetrahymena thermophila*. *Methods Cell Biol.* 109:357–378. http://dx.doi.org/10.1016/B978-0-12-385967-9.00013-X

Wloga, D., and J. Frankel. 2012. From molecules to morphology: cellular organization of *Tetrahymena thermophila*. *Methods Cell Biol.* 109:83–140. http://dx.doi.org/10.1016/B978-0-12-385967-9.00005-0

Wright, R.L., B. Chojnacki, and J.W. Jarvik. 1983. Abnormal basal-body number, location, and orientation in a striated fiber-defective mutant of *Chlamydomonas reinhardtii*. *J. Cell Biol.* 96:1697–1707. http://dx.doi.org/10.1083/jcb.96.6.1697

Yang, J., X. Liu, G. Yue, M. Adamian, O. Bulgakov, and T. Li. 2002. Rootletin, a novel coiled-coil protein, is a structural component of the ciliary rootlet. *J. Cell Biol.* 159:431–440. http://dx.doi.org/10.1083/jcb.200207153